SPATIALLY RESOLVED EMISSION SPECTROSCOPY ALONG A SPT CHANNEL. INTERPRETATION OF DATA BY A COLLISIONAL-RADIATIVE MODEL.

Philippe Leray, Jean Bonnet, Daniel Pigache

ONERA (Office National d'Etudes et de Recherche Aérospatiale)
BP n°72 92322 Châtillon cedex, France
phone: +33 1 69 93 61 70, fax: +33 1 69 93 61 82

Tiberiu Minea, Jean Bretagne, Michel Touzeau

Laboratoire de Physique des Gaz et des Plasmas, U.A. CNRS
Bat. 212, Université Paris-Sud, 91405 ORSAY Cedex, France
phone: +33 1 69 15 78 81, fax: +33 1 69 15 78 44

ABSTRACT

Optical emission spectroscopy was used for a comprehensive approach of microscopic phenomena in a stationary plasma thruster (SPT). A SPT 50 laboratory model (50 mm outer channel diameter) was especially designed to allow the recording of the emission spectra at given locations along the axis of the SPT channel. XeI and XeII spectra have been recorded in pure Xenon for different values of the discharge parameters: flow rate, discharge voltage and magnetic field. Other spectra have been recorded in Xenon-Helium mixture in order to characterize the Electron Energy Distribution Function (EEDF). The interpretation of experimental results on the basis of preliminary results of a collisionnal-radiative model are presented. This model solves a set of kinetics equations taking into account the various processes involved. The comparison of the experimental results with those of the model allow to estimate the shape of the EEDF and to deduce the spatial variations of plasma parameters.

1. INTRODUCTION

The SPT Mark2 thruster has been studied in spectroscopic emission in the SEP laboratories during life time tests in 1994 and 1995 [1]. The plasma emission was observed close to the exit plane of the thruster and in the beam.
The intensity of the light emission along a SPT channel are different according to the value of the local electric field which is weak close to the anode and intense close to the exit plane in the so-called acceleration zone. This preliminary experiment had to be completed by an analysis inside the channel and just outside the exit plane with a good spatial resolution along the discharge axis, we assume that the emission is homogeneous in the radial direction because of the structure of the magnetic field.

2. DESCRIPTION OF THE EXPERIMENT

A SPT prototype, designed and manufactured by the Kurchatov Institute, was settled in a 800 l vacuum tank pumped with a 5000 $l.s^{-1}$ cryogenic pump. This vacuum tank is installed at the Laboratoire de Physique des Milieux Ionisés (Ecole Polytechnique, Palaiseau, France) [2].
Seven identical devices, held by a manual micropositionner, collect the light emitted perpendicularly to the SPT axis. These devices were composed of 4 mm-diameter, 10 mm focal length lenses and 600 µm-diameter U.V grade fused silica optical fibers. The first five devices collect the light through 1 mm diameter holes drilled in the external wall of the SPT with 5 mm spacing (fig.1) which play the role of diaphragms. The last two devices collect the plasma light at 1 and 21 mm, respectively, downstream the exit plane of the thruster. For these two devices the observed zone is larger because of the absence of a hole in the dielectric wall.
Facing the holes in the external surface of the channel other holes have been drilled on the internal surface to trap the light and reduce the reflections on the dielectric surface.
The seven fibers coming from the chamber are introduced, through an adapted entrance, in a JOBIN-YVON spectrometer (model M270). This spectrometer is equipped with three gratings : two 150 gr/mm blazed at 300 nm and 500 nm, and one 600 gr/mm blazed at 500 nm. The width of the slit is set to 10 µm. The output light of the spectrometer is received on a cooled CCD camera (EGG Princeton E130 with light amplifier during the first set of experiments, and OMA4 without light amplifier in the second set). The detection system has a 578 x 578 pixels reception matrix. The light received from the seven optical fibers is distributed on seven distinct stripes on the matrix. Finally the camera is connected to a computer which reads the information through an acquisition software (WINVIEW) (Fig. 2).

The second observation is the modification of the intensity ratio between ionic lines and neutral ones along the thruster channel. This phenomenon can be seen on figure 3 with the neutral line at 467.1 nm and the ionic line at 460.3 nm. The neutral line is more intense than the ionic one before the polar plate and it is the reverse after the polar plate. This confirms that most of the ionization and excitation takes place in the region of high magnetic field near the exit plane.

4. PARAMETRIC STUDY

This study allows to evaluate the influence of the discharge parameters. The parameters studied are the xenon flow rate (8, 9, 9.5, 10, 11 and 12 $cm^3.min^{-1}$), the discharge voltage (250, 300 and 350 Volts) and the value of the magnetic field (through the current intensity in the external coil).
In all these configurations, the variation of the intensity of 16 neutral lines and 8 ionic lines which are free of overlapping have been studied. Along the channel the spectroscopic emission of the plasma presents large variations (fig.3). We will try to interpret these variations by using the model. This study shows that in this range of experimental conditions the main influence is observed when the xenon mass flow rate is varied. Detailed results have been already presented in ref. [10].

5. INTRODUCTION OF HELIUM

The purpose of the introduction of helium was to get information about the population of high energy electrons. The excitation of neutral xenon lines needs electron energies typically above 9.5 eV depending on the lines while for helium lines these energies must be higher than about 20 eV.
During this second set of experiments, the near infrared spectrum was recorded up to 1100 nm, because of the presence of some important lines of XeI and HeI. After some tests, it appeared that up to 10 % (concentration) of Helium, no significant modifications can be seen on the xenon spectra emission and on the discharge current and voltage. For 20 or 30 % the difference appeared only in the beam of the thruster (fig. 4). When the concentration is higher than 30%, the ion beam is still stable, but its color shifts from blue to green.
Seven helium lines are detected (singlets 501.5, 728.1 and triplets 388.8, 447.1, 587.5, 706.5, 1083.0 nm) and are included in this systematic comparison. For an helium partial pressure lower than 10%, HeI lines mentioned above cannot be detected except for the 587.5 nm one.
The variations of Xe and He line intensities along the channel are different. Figure 5 shows three representative examples of XeI, XeII and HeI lines. The main differences are observed between fibers 4 and 6. In this region the growth of the ionic line is more significant than the two others. We can also notice the difference between XeI and HeI lines from fiber 5 to fiber 6 : the XeI line decreases while the HeI line increases.
In order to compare the collisional radiative model results with the experimental ones, a large number of XeI lines were observed : 105 XeI lines which involve the levels taken into account in the model were followed. Helium lines can be easily identified in the spectra because they are proportional to the Helium concentration.

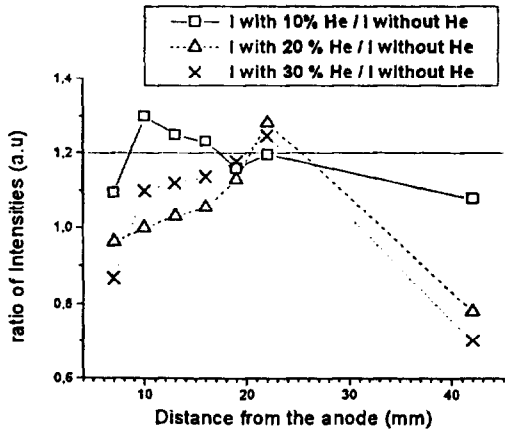

Figure 4. Ratio of XeI line intensities with and without Helium

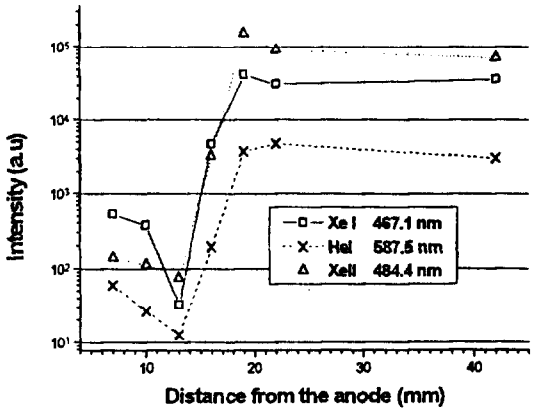

Figure 5. Comparison between light intensities of different species of the plasma with 30 % Helium.

6. COLLISIONAL-RADIATIVE MODEL

The present model was developed on the basis of a previous one by Guimarães *et al.* [3,4], it has been modified to simulate the plasma kinetics in the SPT. This numerical model was adapted to solve the set of kinetic equations relative to excited states of xenon and helium neutral atoms. We consider that the various excited states are produced and quenched by inelastic and superelastic electron-atom collisions, deexcitation is also due to radiative transitions and collisions with walls. In contrast with refs [3,4], we assume a fixed EEDF that we consider as being the sum of two maxwellian distributions with two sets (N_{e1},) and (N_{e2}, T_{e2}) of electron densities and temperatures with $T_{e1} < T_{e2}$.

The master equations to solve are the following:

$$\frac{dN_i}{dt} = \sum_j C^e_{ji} . N_i . n_e + \sum_{j>i} A_{ji} . N_j$$

$$- N_i \left(\sum_j C^e_{ij} . n_e + \sum_{j<i} \left(1 - \Lambda_{ij}\right) . A_{ij} + C^e_{ion,i} . n_e \right)$$

$$\pm \sum_{il} k^{hp}_{il} . N_k . N_l - g_i \frac{N_i}{t_i}$$

where $C^e_{ji} = \int v . f(u) \sigma_{ji}(u) du$ is the electronic excitation or de-excitation coefficient for the transition $j \rightarrow i$ and $C^e_{ion,i}$ the ionization coefficient of level *i*. *f(u)* is the distribution function (EEDF) normalized to 1. σ_{ij} is the electron impact cross section for the transition $i \rightarrow j$. A_{ij} is the Einstein coefficient for the transition i $\rightarrow$ j. We eventually take into account the self-absorption by introducing a calculated factor (1 - Λ_{ij}). k^{hp}_{il} is the coefficient of collisions between heavy particles *k* and *l*. τ_i is the effective transit time for diffusion of metastable state *i* to the walls and γ_i the corresponding destruction probability on these walls.

For the model, it is then necessary to know the electron collision cross sections involving the xenon and helium levels. This set of cross sections has been constructed from various sources. First, the excitation cross-sections from the ground state atoms are from Puech *et al*[5] for xenon, and from the compilation of Gousset *et al*[6] for helium. Second, experimental data from various references are used to characterize the ionization process from excited levels and some transitions between excited levels. Third, the missing electron collision cross sections are introduced from Drawin empirical formula[7]. The data for radiative transitions (transition probabilities, oscillator strengths) are from refs [8,9].

The physical conditions (pressure, geometry,...) introduced in the model correspond to the thruster channel. Unless specified, the neutral xenon density was taken to be $2.7.10^{13}$ cm^{-3}.

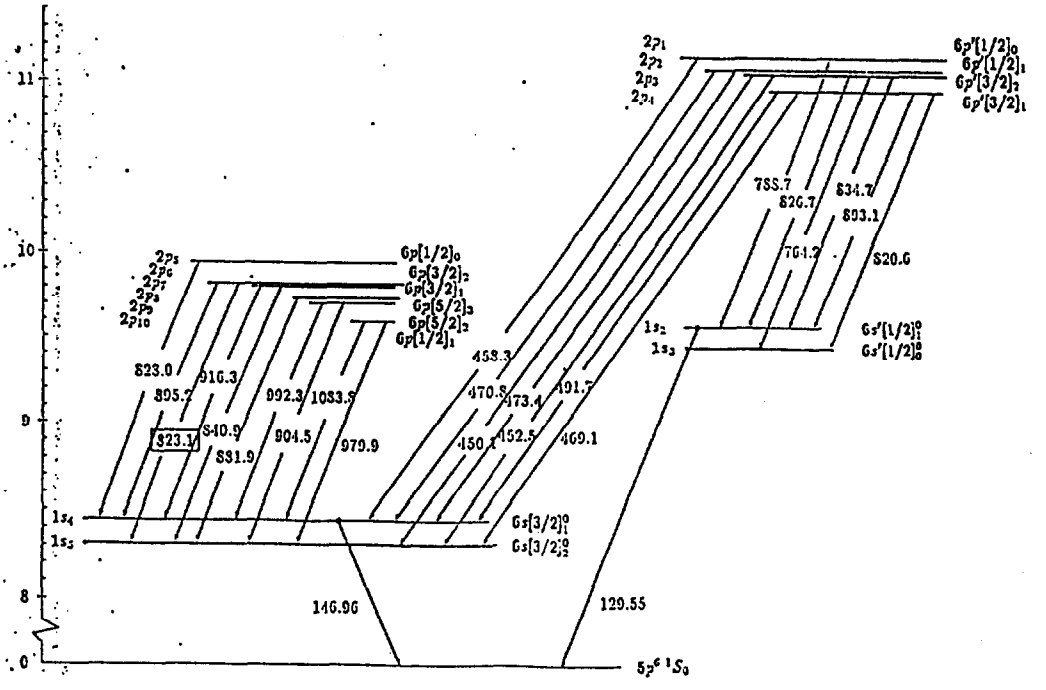

Figure 6. Energy diagram of Xe I levels involved in the line emissions used here.

First, different tests were made with a maxwellian electron energy distribution and 1% of Helium, with various temperatures (2, 3, 4, 6 and 10 eV) and densities (10^{11}, 10^{12}, 10^{13}, 10^{14} and 10^{15} cm^{-3}). We particularly studied the different pathways for the excitation in XeI and HeI states. The relative importance of the various processes (radiative transitions, inelastic and superelastic collisions,...) were discussed. The corresponding results and conclusions of this preliminary study are reported in ref.[10].

Ten Xenon neutral lines are considered :

820.6 nm	$2p_4 \rightarrow 1s_3$
473.4 nm	$2p_3 \rightarrow 1s_4$
450.1 nm	$2p_2 \rightarrow 1s_5$
893.0 nm	$2p_4 \rightarrow 1s_2$
895.2nm	$2p_6 \rightarrow 1s_4$
764.2 nm	$2p_2 \rightarrow 1s_3$
979.9 nm	$2p_{10} \rightarrow 1s_5$
828.0 nm	$2p_5 \rightarrow 1s_4$
840.9 nm	$2p_7 \rightarrow 1s_4$
1083.8 nm	$2p_{10} \rightarrow 1s_4$

and 6 helium lines :

447.1 nm	$4^3D \rightarrow 2^3P$
587.5 nm	$3^3D \rightarrow 2^3P$
667.8 nm	$3^1D \rightarrow 2^1P$
706.5 nm	$3^3S \rightarrow 2^3P$
728.1 nm	$3^1S \rightarrow 2^1P$
1083.0 nm	$2^3P \rightarrow 2^3S$

Before presenting results of the model and the comparison with the experimental data, let us emphasize the role of the various classes of electrons. Referring to the EEDF, three energy domains can be schematically defined :

- low-energy electrons (energies of a few eV) which yield redistribution of populations between excited levels in Helium and Xenon.
- electrons with intermediate energy (higher than 8 eV) which determine the excitation from the Xenon fundamental level.
- electrons with energies higher than 20 eV which determine the excitation from the Helium ground state.

In the model, we used an EEDF defined as the sum of two maxwellian distributions. Comparisons have been made for results with 10% of Helium.

A first step was to consider the redistribution of populations of excited states to deduce the electron density. In figures 7 and 8 we present the intensities ratio for some pairs of XeI and HeI lines respectively. Results for HeI lines and for fibers near the anode are too weak to be reported. Experimental data are presented with error bars.

7. INTERPRETATION OF EXPERIMENTS

In the comparison between model and experiment, we used the lines emitted from 6p and 6p' xenon levels because their spectroscopic data and their excitation cross sections by electron collisions are relatively well known. In the case of Helium, the choice is restricted because of the limited number of lines which were detected in the spectra.

Our discussion will be developed in three steps.

First, we can then make a comparison of experimental ratios against calculated ratios which are illustrated by figures 9 and 10 which give the calculated intensity ratios of pairs of XeI and HeI lines, respectively, versus the density N_{e1} of cold maxwellian electrons. Helium data are probably more reliable in terms of electron cross sections than xenon ones and, in addition, we can assume that helium remains weakly ionized in this discharge. So, we preferably used helium data. Results of Fig. 10 compared to each data reported in Fig.8 permits to determine the electron density N_{e1} for the various fibers (at various distances from the anode)

Second, we compare experimental intensity ratio for pairs of xenon lines to corresponding calculated ratios. Identically to helium we compare Fig. 7 to Fig. 9. This test does not give more information for N_{e1}, but it permits to validate the model for xenon. Table 1 presents the values of N_{e1} determine by this method for the different fibers.

It should be noted that the calculations have been performed for different values of Te_1 between 1 and 10 eV. It results that the best fit is obtained for a value of T_{e1} between 2 and 5 eV.

Third, to determine the high energy population of electrons, we compare ratios of helium line intensities to xenon line ones. These ratios were found to be very sensitive to the parameters N_{e2} and T_{e2} corresponding to hot electrons.

Figure 11 shows experimental data of these ratios for the fibers 4 to 7 (beam). Because of the weakness of helium lines we could not determine these ratios for fibers 1 to 3. However, we can note the large variation of experimental data between the different fibers.

Experimental results are then to be compared to results of the model. In figures 12, 13 and 14, we show the calculated ratios versus N_{e2} for three electron temperature. These temperatures are respectively 5, 10 and 20 eV. For 30 eV and more the results are equivalent to those obtained for 20 eV.

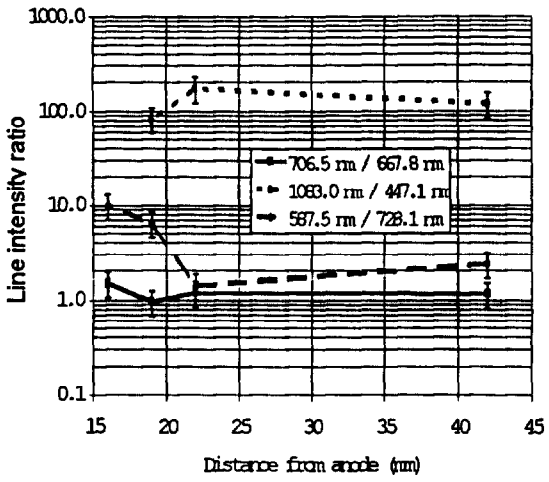

Figure 7. Experimental ratios of some Helium lines.

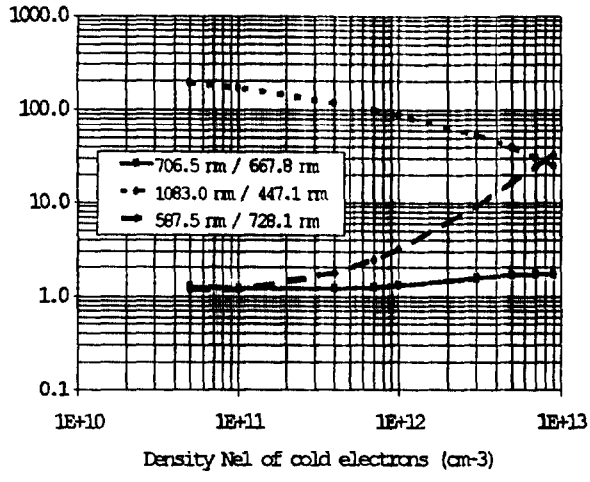

Figure 8. Helium calculated ratios intensities versus Ne_1 for Te_1=2eV. Other parameters are $N_{e2}=3.10^{11}cm^{-3}$; T_{e2}=10eV ; [Xe] =$2.75.10^{13}$ cm^{-3} [He] = 2.75 10^{12} cm^{-3}..

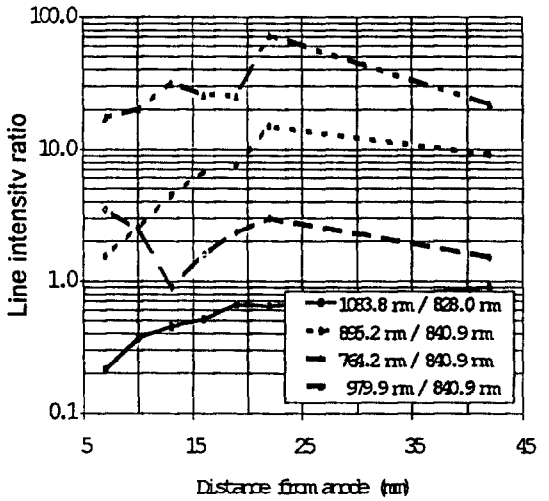

Figure 9. Experimental ratios of some Xenon lines.

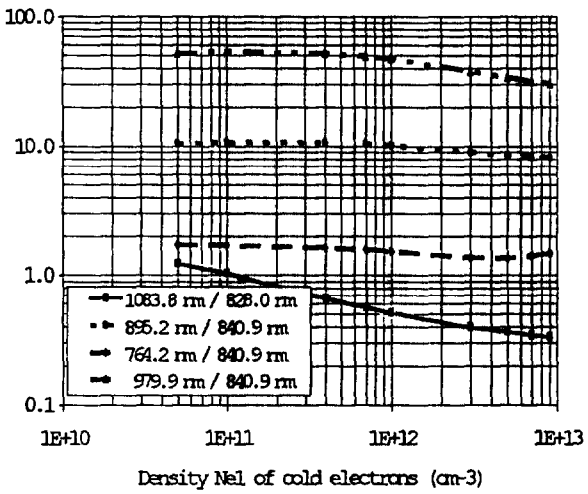

Figure 10. Xenon calculated ratios intensities versus Ne_1 for Te_1=2eV. Other parameters are $N_{e2}=3.10^{11}cm^{-3}$; T_{e2}=10eV ; [Xe] =$2.75.10^{13}$ cm^{-3} [He] = 2.75 10^{12} cm^{-3}.

Fiber Number	N_{e1} from intensity ratios of XeI lines	N_{e1} from intensity ratios of HeI lines
1 (anode)	2.10^{11}-2.10^{12} cm^{-3}	No data
2	2.10^{11}-2.10^{12} cm^{-3}	No data
3	7.10^{11}-3.10^{12} cm^{-3}	No data
4	4.10^{11}-2.10^{12} cm^{-3}	2.10^{12}-4.10^{12} cm^{-3}
5	10^{12}-3.10^{12} cm^{-3}	10^{12}-3.10^{12} cm^{-3}
6	2.10^{11}-7.10^{11} cm^{-3}	5.10^{10}-5.10^{11} cm^{-3}
7 (beam)	3.10^{11}-10^{12} cm^{-3}	3.10^{11}-6.10^{11} cm^{-3}

Tab 1. Electron density deduced from line intensity ratio.

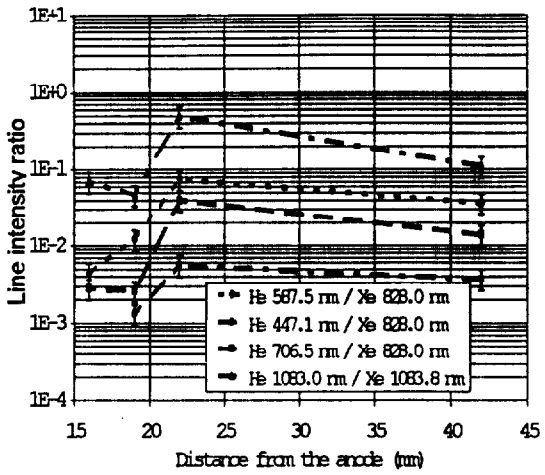

Figure 11. Experimental ratios of helium line to Xenon line intensities.

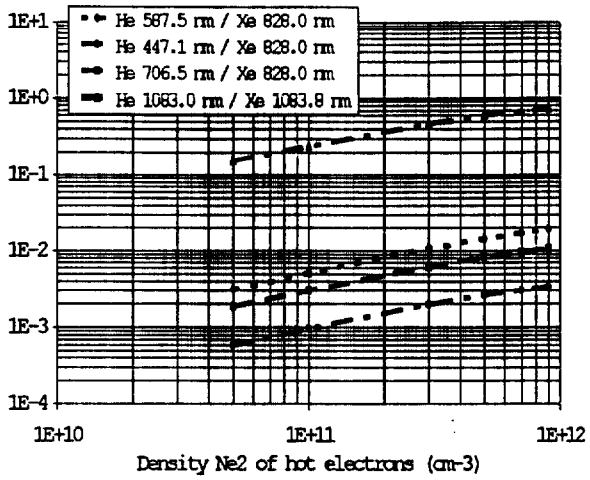

Figure 12. Calculated ratios of helium line to Xenon line intensities versus N_{e2} for Te_2=5eV. Other parameters are $N_{e1}=10^{12}cm^{-3}$; T_{e1}=2eV; [Xe] = [He] = 2.75 10^{12} cm^{-3}.

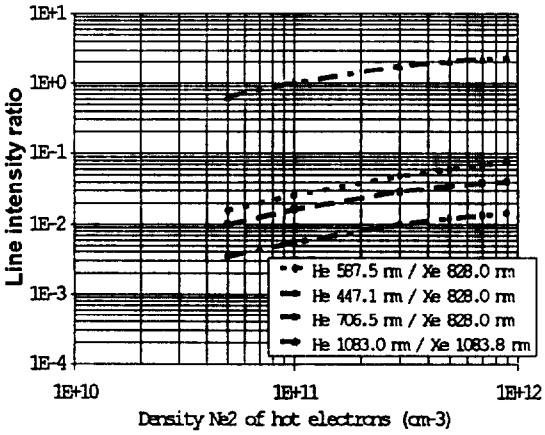

Figure 13. Calculated ratios of helium line to Xenon line intensities versus N_{e2} for T_{e2}=10eV. Other parameters are $N_{e1}=10^{12}cm^{-3}$; T_{e1}=2eV; [Xe] = [He] = 2.75 10^{12} cm^{-3}.

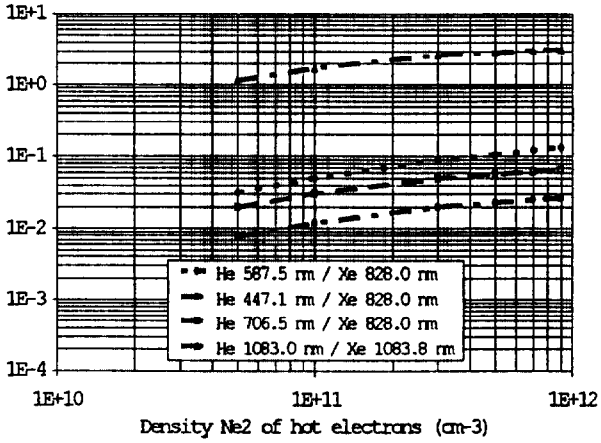

Figure 14. Calculated ratios of helium line to Xenon line intensities versus N_{e2} for Te_2=20eV. Other parameters are $N_{e1}=10^{12}cm^{-3}$; T_{e1}=2eV; [Xe] = [He] = 2.75 10^{12} cm^{-3}.

For fibers 6 and 7, it has been necessary to take into account of the value of the ionization degree for xenon. The results shown on Figs. 12-14 are calculated for an ionization of xenon of 90%. For neutral xenon, the input concentration is divided by ten, at the same time the neutral helium density is considered as being the input one. It must also be noted that a significant difference between T_{e1} and T_{e2} is needed to achieve a coherence between experimental and theoretical results.

At this stage, it seems to be difficult to determine an unique solution for the three parameters N_{e2}, T_{e2} and [He]/[Xe]. It remains that some results of the model cannot match with the experiment for instance as mentioned above, for fibers 6 and 7 when we do not consider a realistic ionization degree for xenon. A systematic study of the influence of all of the parameters is actually in progress. We calculate the variation of the ratios presented here against N_{e2} for different conditions given by T_{e2} (5, 10 and 20 eV) and ionization degree (0, 33, 66, 90 and 95 %). Other experimental results such as the relative spatial variations of each of the XeI and HeI lines can also be used. Even if the solution is not unique, we can guess to find for each fiber and each experimental condition a restricted set of solutions which appear to be more realistic and compatible with all experimental results. These solutions have also to be compared with measurements made by other laboratories.

8. CONCLUSION

We have presented experimental results for the spatial variations of the optical emission of the plasma in pure xenon and with addition of helium for a SPT 50 thruster. The introduction of Helium up to 10% does not perturb significantly the plasma. Helium lines were clearly seen, so it is possible to use these emission lines together with those emitted by xenon to deduce information about the plasma parameters.

In parallel to the experiment we developed a collisional-radiative model for the xenon and xenon/helium plasma. We show that the redistribution of populations between excited levels of a given element (XeI or HeI) leading to important modifications of the relative intensities of lines permit to determine the value of electron density. This result was only possible with a detailed description, in the model, of the kinetics of excited levels involved in the spectral emissions detected in the experiments. The use of HeI to XeI intensity ratios yield preliminary results on the ionization degree and on the shape of the EEDF.

We demonstrate the interest of spatially resolved OES for the determination of plasma parameters. Despite the fact that more work is still necessary to analyze all the experimental results, we can conclude that the method of introducing helium, as a minority component, can lead to an estimation of the electron density and useful information about plasma parameters and about the shape of EEDF.

This work has been performed in the frame of the Groupement de Recherche CNRS-CNES-SEP-ONERA 1184 "Propulsion à Plasma pour Systèmes Orbitaux".

8. REFERENCES

[1] Leray Ph., Bonnet J., Pigache D., Bretagne J. and Ricard A. 1995 24th IEPC, Moscow, IEPC-95-192.

[2] Guerrini G., Michaut C., Dudeck M., and Bacal M.,

[3] Guimarães F. and Bretagne J. 1993 Plasma Sources Sci. Technol. **2** 127.

[4] Guimarães F., Almeida J.B., and Bretagne J. 1993 Plasma Sources Sci. Technol. **2** 138.

[5] Puech V. and Mizzi S. 1991 J. Phys. D: Appl. Phys. **24** 1974.

[6] Alves L.L., Gousset G., Ferreira C.M. 1992 J. Phys. D: Appl. Phys. **25** 1713.

[7] Drawin H. W. 1967 E.U.R-C.E.A-F.C Report 383.

[8] Aymar M. and Coulombe M. 1978 Atom. Data Nucl. Data Tables **21** 540.

[9] Miller M. H. and Roig A. R. 1973 Phys. Rev. A **8** 480.

[10] Leray P., Bonnet J., Pigache D., Bretagne J., Minea T., Touzeau M., Proceeding of the 2nd ESPC, Noordwijk, 27-29 May 1997 (to be published)